FOI-R--1092--SE
December 2003
ISSN 1650-1942
Technical report

Patrik Hermansson

A Semi-Empirical IR Signature Model for Tilted Surfaces

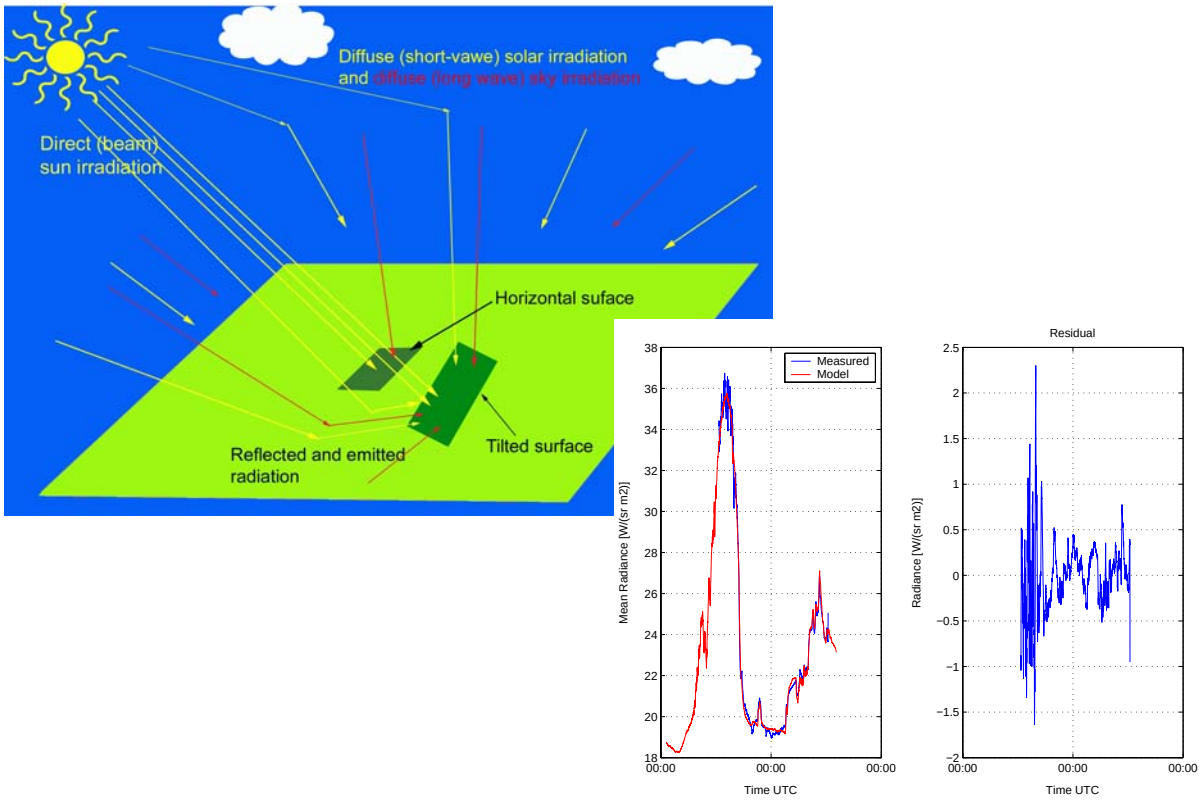

Sensor Technology
SE-581 11 Linköping

SWEDISH DEFENCE RESEARCH AGENCY

Sensor Technology
P.O. Box 1165
SE-581 11 Linköping

FOI-R--1092--SE

December 2003

ISSN 1650-1942

Technical report

Patrik Hermansson

A Semi-Empirical IR Signature Model for Tilted Surfaces

Issuing organization	Report number, ISRN	Report type
FOI – Swedish Defence Research Agency Sensor Technology P.O. Box 1165 SE-581 11 Linköping	FOI-R--1092--SE	Technical report
	Research area code 6. Electronic Warfare	
	Month year December 2003	**Project no.** E30161
	Customers code 5. Commissioned Research	
	Sub area code 62 Stealth Technology	

Author/s (editor/s)	Project manager
Patrik Hermansson	Claes Nelsson
	Approved by Lars Bohman
	Sponsoring agency Armed forces
	Scientifically and technically responsible

Report title

A Semi-Empirical IR Signature Model for Tilted Surfaces

Abstract (not more than 200 words)

In this document we present the further development that has been made of a previously presented semi-empirical model for calculation of thermal IR signatures from background elements. An improved modelling of non-horizontal surfaces has been included in the semi-empirical model. The model has been tested by curve-fitting the model to time histories of measured LWIR radiance from two flat, tilted panels. The two panels have different coatings with significantly different emissivities in the infrared. The correspondence between the curve-fitted model and measurements is very good for both panels during the entire time period for which we have measurements. For the purpose of future evaluation we also present simple models for latent heat and precipitation which have been included in the semi-empirical model. It is concluded that the developed semi-empirical model could be a useful tool in several applications of IR-signature prediction and simulation. It is also noted that a continued development and, in particular, validation of the model would be of value.

Keywords

modelling, semi-empirical, IR, signature, atmospherical

Further bibliographic information	Language English
ISSN 1650-1942	**Pages** 39 p.
	Price acc. to pricelist

Utgivare	Rapportnummer, ISRN	Klassificering
Totalförsvarets Forskningsinstitut - FOI	FOI-R--1092--SE	Teknisk rapport
Sensorteknik	**Forskningsområde**	
Box 1165	6. Telekrig	
581 11 Linköping	**Månad, år**	**Projektnummer**
	December 2003	E30161
	Verksamhetsgren	
	5. Uppdragsfinansierad verksamhet	
	Delområde	
	62 Signaturanpassning	

Författare/redaktör	Projektledare
Patrik Hermansson	Claes Nelsson
	Godkänd av
	Lars Bohman
	Uppdragsgivare/kundbeteckning
	Försvarsmakten
	Tekniskt och/eller vetenskapligt ansvarig

Rapportens titel (i översättning)

En semi-empirisk IR-signaturmodell för lutande ytor

Sammanfattning (högst 200 ord)

En tidigare presenterad semi-empirisk modell för beräkning av IR-signatur från bakgrundselement har vidareutvecklats för att bättre kunna prediktera radians från icke-horisontella ytor. Modellen har testats genom att kurvanpassa modellen mot uppmätt radians i LWIR från två lutande plana paneler. De två panelerna har ytbeläggningar med avsevärt olika emissivitet i IR-området. Överensstämmelsen mellan den kurvanpassade modellen och uppmätta data är god för båda panelerna och för hela den tidsperiod som vi har mätdata. Förenklade modeller för värmeöverföring via nederbörd samt avdunstning och kondensation har också implementerats i den semi-empiriska modellen. Den semi-empiriska modellen kan bli ett värdefullt verktyg i ett flertal tillämpningar av signaturprediktion i det termiska IR-området. Behovet av fortsatt utveckling och, i synnerhet, validering av den semi-empiriska modellen noteras också.

Nyckelord

modellering, semiempirisk, IR, signatur, atmorsfärseffekter

Övriga bibliografiska uppgifter	**Språk** Engelska
ISSN 1650-1942	**Antal sidor:** 39 s.
Distribution enligt missiv	**Pris: Enligt prislista**

1 INTRODUCTION

Models for calculating infrared (IR) signatures from targets and backgrounds are useful tools in assessment and management of IR signatures. In the thermal infrared the contrast between different elements in a scene can change considerably in magnitude, and sometimes also rapidly, over a period of time. Variations in the environmental conditions (for instance changes in weather conditions) can cause changes in the contrast between elements in a scene. By performing measurements of thermal IR signatures, reliable data can be obtained for some environmental conditions. Modeling of IR signatures is a way to assess temporal aspects of IR signatures for a larger range of environmental conditions than actual measurements cover.

A number of coupled physical phenomena have to be considered in modeling of thermal IR signatures. Modeling of heat transfer, atmospheric effects and radiometry are all needed in order to calculate the in-band radiance detected by an IR sensor. There are a large number of models and methods, with varying degrees of complexity and accuracy, for calculating the individual physical processes involved in modeling of IR signatures from targets and backgrounds. The commercial programs which are available for prediction of IR signatures can roughly be divided into programs for calculation of IR signatures from individual objects (usually targets) and programs developed for calculation of IR signatures from entire scenes with background and targets. Due to the great complexity involved in modeling IR signatures the models used in (commercial) signature prediction programs are usually adapted to the main area of application of the program. For instance, the IR scene simulation programs usually only consider one-dimensional heat transfer while programs specialized on calculating thermal signatures from vehicles often solve the conduction heat transfer problem in three dimensions.

Models and computer programs for prediction of thermal IR signatures often require large amounts of input parameters, such as thermophysical material parameters, and the work needed to properly assign values to these parameters should not be underestimated. In a semi-empirical model, on the other hand, the thermophysical parameters quantifying the heat transfer mechanisms of a considered background or surface element are determined by curve-fitting the model to time histories of measured element radiance or surface temperature.

In Ref 1 we presented the initial results from the development of a semi-empirical model for calculation of thermal IR signatures from background elements. Here we will present some further developments of this model. In particular, the model is developed further to calculation of thermal IR signatures from non-horizontal surfaces.

In Section 2 we begin by recapitulating the semi-empirical model presented in Ref 1 and in the succeeding sections we present new developments with results and examples in Section 7.

2 SEMI-EMPIRICAL MODEL FOR HORIZONTAL SURFACES

In this section we will recapitulate the semi-empirical model for calculation of radiance from horizontal surface elements in Ref 1, where the model was applied to calculation of the radiance from different types of background elements, such as patches of grass, trees and asphalt. The same model with a slight modification has also been applied to calculation of the temperature difference between air and background in Ref 2. In Ref 1 no details on the derivation of the semi-empirical model were presented. Therefore, we present the derivation

(and the approximations and assumptions used therein) of the semi-empirical model equations in more detail in Appendix A.

2.1 DERIVATION OF THE SEMIEMPIRICAL ALGORITHM

The model in Ref 1 is based on an efficient one-dimensional, time dependent (non-steady-state) equation for calculation of the surface temperatures of a flat surface element. Using a one-dimensional heat transfer model means that heat only is transferred in the perpendicularly to the flat surface. The equation which is the starting point of our model describes the heat balance over the surface and it can be written as (Ref 3 and Ref 4)

$$\frac{dT_s}{dt} = \frac{k_1}{\rho c d}\left[\Phi_{sun} + \Phi_{sky} + \Phi_{emiss} + \Phi_{conv}\right] - \frac{k_2}{P_e}(T_s - T_0) \tag{1}$$

where T_s is the surface temperature, t is time and the square bracket term on the right hand side describes the heat transfer to and from the surrounding above the surface and the term proportional to $T_s - T_0$ describes the heat transfer through conduction to a layer "deep" below the surface. In Eq. (1) the parameter ρ is the density, c is the specific heat, d is proportional to the depth reached by the diurnal temperature wave, P_e is the period of one day, T_0 is a (thermally) "deep" layer temperature which is constant and k_1 and k_2 are dimensionless constants. The heat fluxes, Φ_{***} , which are included in Eq. (1) are given by

$$\begin{aligned}
\Phi_{sun} &= \alpha_{sun} E_{sun} \\
\Phi_{sky} &= \varepsilon E_{sky} \\
\Phi_{emiss} &= -\varepsilon \sigma T_s^4 \\
\Phi_{conv} &= -h(v)(T_s - T_a)
\end{aligned} \tag{2}$$

where

E_{sun} : (short - wave) solar irradiance on the surface
E_{sky} : (long wave) sky irradiance on the surface
α_{sun} : (short - wave) solar absorptivity
ε : (long wave) emissivity
v : wind speed
$h(v)$: convection factor chosen as $h(v) = a_1 + a_2 v^{0.7}$ where a_1 and a_2 are constants
T_a : air temperature

In Figure 1 we illustrate the heat fluxes over the surface which are considered in Eq. (1). The conduction heat transfer to the deep layer with temerature T_0 is in Eq. (1) through a single homogeneous material. However, the thermal material parameters entering the equation can also be viewed as as "effective material parameters" for more complex material structures, making the model approximately valid also for some combinations of materials. We take advantage of this in our semi-empirical anzats where "effective material parameters" are curve fitted to measured data.

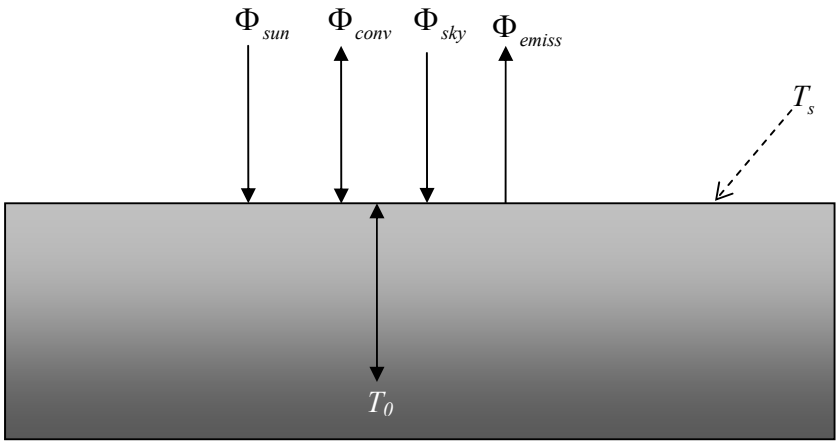

Figure 1 Heat fluxes considered in the 1-dimensional thermal equation.

By linearizing the T_s^4 term in Eq. (1) about for instance T_0 we obtain a linear first order ordinary differential equation which can be solved by standard methods as (see Appendix A). However, in optical signature applications, which is our area of interest, it is the radiance, L, (or possibly the related quantity of apparent temperature) in some wavelength band that is of interest. Furthermore, we like to arrive at an expression in which unknown material and model parameters can be determined through, preferably linear, cure-fitting of the model to measurements and in our applications it s usually the in-band radiance that has been measured and not the actual surface temperature. As is described in Appendix A, we can from Eq. (1) derive the following approximate expression for the in-band radiance (primarily LWIR), $L(t)$, from the considered surface element (atmospheric absorption of radiance between surface and sensor excluded):

$$L(t) \approx \int_{t_0}^{t} \left[\sum_{i=1}^{N} A_i e^{-B_0(t-s)} P_i(s) + \sum_{j=1}^{M} C_j P_j(s) \delta(t-s) \right] ds + D \qquad (3)$$

where $N = 4$, $M = 2$, $\delta(\bullet)$ is the Dirac delta function, $P_1 = E_{sun}$, $P_2 = E_{sky}$, $P_3 = T_a$, $P_4 = T_a v^{0.7}$ and the parameters B_0, A_1, A_2, A_3, A_4, C_1, C_2 and D are combinations of the thermo-physical constants in Eq. (1). In the derivation of Eq. (3) we have used some simplifying assumptions and approximations as described in Appendix A. It is assumed in the derivation that t_0 is "much smaller" than t and that the mean value of the wind speed can be considered to be constant for large times. For the ordinary surfaces and ground elements which often have time constants in the order (or less) of hours, "much smaller" means times in the order of at most a few days. It is also, for instance, assumed that the surface emits and reflects radiation diffusely.

In Appendix A it is shown that an incremental algorithm for $L(t)$ can be derived from Eq. (3). The derivation is based on discretizing the integral for piecewise constant conditions (piecewise constant P_i's). For later use we show the result for $\{N, M : N \geq M \geq 0\}$ in Eq. (3):

$$L(t+\Delta t) = aL(t) + \sum_{i=1}^{N} b_i \overline{P}_i^{t+\Delta t} + \sum_{i=1}^{M} c_i P_i(t+\Delta t) + d \tag{4}$$

where Δt is the time increment and

$$\begin{aligned}
a &= e^{-B_0 \Delta t} \\
b_i &= -e^{-B_0 \Delta t}\left(\frac{A_i}{B_0} + 2C_i\right) + \frac{A_i}{B_0}, \quad && i \le M \\
b_i &= \frac{A_i}{B_0}\left(1 - e^{-B_0 \Delta t}\right), && M < i \le N \\
c_i &= C_i(1 + e^{-B_0 \Delta t}), && i \le M \\
d &= D(1 - e^{-B_0 \Delta t}) \\
\overline{P}_i^{t+\Delta t} &= (P_i(t+\Delta t) + P_i(t))/2
\end{aligned} \tag{5}$$

2.2 APPLICATION TO HORIZONTAL SURFACES AND BACKGROUNDS

We will now outline how Eqs. (4) and (5) can be applied to horizontal surfaces (and some other background types) using measured weather data and measured radiances as was done in Ref 1.

Suppose that we have measurements of the radiance, $L(t)$, (corrected for atmospheric effects as in Ref 1) from a horizontal surface and that we also have measurements of the weather parameters E_{sun}, E_{sky}, T_a and v at times t_1, $t_1, t_1 + \Delta t, \ldots, t_1 + n\Delta t_1$, where $n+1$ is the number of measurements and we assume that $n >> N + M + 2 = 8$. Then it is possible to curve-fit Eq. (4), using linear linear regression, to the measurement data and thereby quantifying the $N + M + 2 = 8$ unknowns a, b_1, b_2 ,b_3 ,b_4, c_1, c_2 and d. In the regression it is assumed that the terms on the right hand side of Eq. (4) are independent. Once the unknown parameters have been determined through linear regression, Eqs. (4) and (5) can be used as a model for predicting the radiance from the type of surface elements that the regression was performed under other weather conditions.

The weather parameters, E_{sun}, E_{sky}, T_a and v, are usually measured using a weather station. Then it is important that the weather parameters are measured in such a way that they are compatible with the model and the surfaces of interest. This for instance means that the weather parameters should be measured in close proximity to the surface for which we like to calculate the radiance. Furthermore, the type of weather station we use (a Vaisala Milos 500) measures the global (short-wave, 0.3-2.8 μm) irradiance and the (long wave, 3.5-40 μm) sky irradiance on horizontal plates facing upwards. This means that we identify E_{sun} with the measured global irradiance and E_{sky} with the measured sky irradiance, provided that the considered surface element is horizontal. Throughout the report we will refer to irradiance on a horizontal surface as *horizontal irradiance*. Here we of course also assume that whenever the sensors on the weather station are in shadow, so is the surface element (i.e. again a condition of "proximity). Weather parameters which are measured by the weather station, and sensor specifications, are shown in Table 1.

Table 1 Weather station parameters and sensors

Weather parameter	Unit	Sensor specification
Wind direction	Degrees	Vaisala WAV15A
Wind speed	m/s	Vaisala WAA15A
Air temperature	°C	Vaisala HMP45D
Relative air humidity	%	Vaisala HMP45D
Air pressure	hPa	Vaisala PTB200A
Visibility	Km	Vaisala FD12P
Extinction coefficient	km^{-1}	Vaisala FD12P
Precipitation	ON/OFF	Vaisala DRD11A
Type of precipitation	Rain/snow	Vaisala FD12P
Intensity of precipitation	mm/h	Vaisala FD12P
Rain accumulation	Mm	Vaisala FD12P
Snow accumulation	Mm	Vaisala FD12P
Present weather	NWS codes	Vaisala FD12P
Global radiation (0.3 - 2.8 μm)	W/m^2	Kipp & Zonen CM 7B
Reflected radiation (0.3 - 2.8 μm)	W/m^2	Kipp & Zonen CM 7B
Sky radiation (3.5 – 40 μm)	W/m^2	Eplab PIR.
Ground radiation (3.5 – 40 μm)	W/m^2	Eplab PIR

In Ref 1 the semi-empirical model was curve-fitted to measurements of weather parameters and mean radiances (corrected for atmospheric effects) from different types of background patches in a LWIR (long wave infrared) wavelength band (≈8-12 μm) and a MWIR (mid wave infrared) wavelength band (≈3-5 μm). Using these fitted parameters, the radiance was calculated and compared with the measured radiance. The results showed rather good agreement between measured and predicted radiance for most of the considered background area elements and the results were in general better in LWIR than in MWIR. The reason for LWIR being predicted better than MWIR is explained mainly by the facts that our semi-empirical model is basically a thermal model and the modeling of reflected radiation is rather crude. Furthermore, the MWIR wavelength band does not correspond well to neither the sun irradiance wavelength band nor the sky irradiance wavelength band measured by the weather station. It should be noted that the accuracy of the model was rather good for the mean radiance from a tree background. Trees have very complex geometry and cannot be considered to be a horizontal surface but still the semi-empirical model (as described above) can be applied to such background elements. In Ref 1, the semi-empirical model was also applied to calculation of the radiance from a vertical wall of a caisson. For this case the agreement between model and measurements was not so good. The reason for this is of course that the wall is not a horizontal surface. In the next Section we will present how we adapt the semi-empirical so that tilted (non-horizontal) surfaces can be treated.

3 SEMI-EMPIRICAL MODEL FOR TILTED SURFACES

In order to apply the semi-empirical model in Ref 1, here reviewed in Section 2.1, we need (amongst other things) measured time histories of short-wave (solar) irradiance and long wave (sky) irradiance on the considered surface as input data. The equipment we use (the weather station) measures short-wave irradiance and long wave irradiances on horizontal plates. As was explained in the previous section, we can then directly use the measured irradiances

provided that the considered surface is horizontal. The irradiances on non-horizontal surfaces, on the other hand, do not in general agree with the irradiances measured with the weather station. However, as we will show in this section, we can, using some models and assumptions, calculate an approximate value of the irradiance on a tilted surface from the measured radiations and then the semi-empirical model in Section 2.1 is applicable.

3.1 SOME USEFUL CONCEPTS

To solve our problem we will make use of some concepts that will be briefly explained here. The solar radiation incident on a surface at ground level is affected by a number of mechanisms. Part of the power incident on a surface is removed by scattering or absorption by air molecules, clouds and other particles in the atmosphere. The radiation that is not reflected or scattered and reaches the surface directly is called **beam radiation**. The radiation which is scattered in the atmosphere is called **diffuse (sun) radiation**. Some radiation can also be **reflected** from the surrounding ground onto the considered surface. The total radiation consisting of these three contributions is called the **global radiation**. In Figure 2 we schematically illustrate the different components of radiation incident on surfaces.

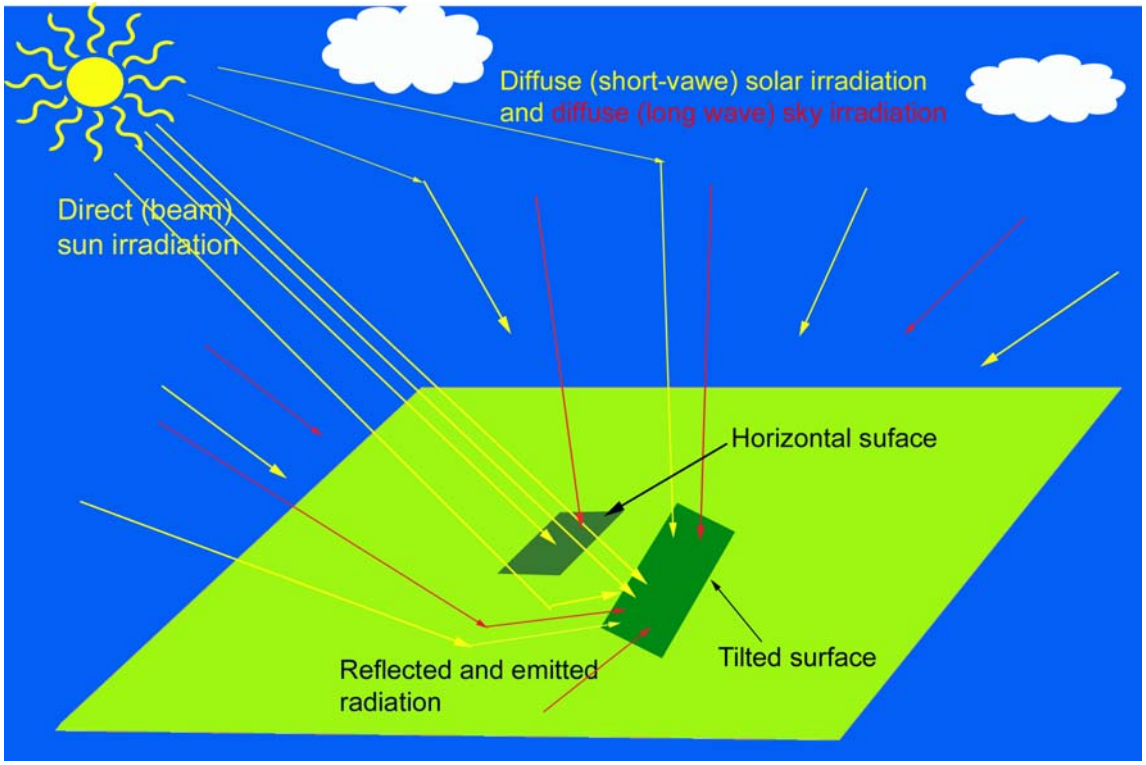

Figure 2 Components of the global radiation incident on surfaces.

We will assume that the long wave sky irradiation is isotropic over the sky hemisphere. Furthermore, we will assume that the ground that surrounds the considered surface reflects radiation diffusely.

We will introduce one more concept which we will use, namely the **clearness index**, K_c (see for instance Ref 5). The clearness index is calculated from the portion of available sun radiation that reaches the ground. More formally the clearness index is defined as the ratio of the measured total (beam and diffuse) solar radiation incident on a horizontal surface at

ground level to the corresponding quantity at the top of the earth's atmosphere as calculated from the solar constant:

$$K_c = E_{sun}^{gh} / E_0 \qquad (6)$$

where E_{sun}^{gh} is the global (here beam and diffuse) sun irradiance on a horizontal surface at ground level and E_0 is the (here global=beam) sun irradiance on a horizontal surface at the top of the earth's atmosphere as calculated from the solar constant. The solar constant is defined as the irradiance (flux density) on a surface perpendicular to the solar beam outside the Earth's atmosphere and it has been measured to be $S_0 = 1367\,\mathrm{W/m^2}$. If the solar elevation (relative to the horizon) at a particular time of day is β_s, see Figure 3, then E_0 is given by:

$$E_0 = S_0 \max(\sin\beta_s, 0) \qquad (7)$$

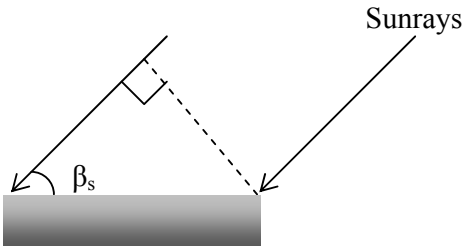

Figure 3 Sunrays (beam radiation) incident on a horizontal surface at solar elevation β_s.

3.2 CALCULATION OF BEAM AND DIFFUSE SUN RADIATION

In order to calculate the irradiance on a tilted surface from measured global irradiance on a horizontal surface we first need to separate the measured global radiation into beam and diffuse radiation. As we mentioned in Section 3.1, scattering of radiation in the atmosphere is a complicated process which require sophisticated modeling if the detailed physics of the scattering process is considered. Furthermore, a detailed modeling of scattering over a period of time requires that changes in cloud cover and cloud type have been monitored during the considered time period. Such physics based modeling of scattering and transmission is beyond the scope of our semi-empirical model and also it would make it more cumbersome to use and numerically more expensive in computing times. We have therefore chosen to take an empirical approach to scattering and calculation of the time-dependent diffuse component of measured global radiation. For, in particular, solar energy applications, empirical correlations have been developed for calculation of the horizontal diffuse radiation from measurements of global horizontal radiation (see Ref 6). Many of these are one-parameter correlations, where the single parameter is the clearness index as defined in Eq. (6). In the literature, correlations for monthly, weekly, daily and hourly time averaged irradiances can be found. There could be an influence of the geographical location on the correlation but it has not (as far as we know) been clearly shown (see Ref 5 and Ref 6 for more on this). We have made no attempt to evaluate all the correlations found in the literature to find the best or the one most suited for our applications. However, since we like to calculate the "instantaneous" (at least time periods less than an hour) diffuse and beam solar irradiances we have chosen a correlation derived for

prediction of hourly horizontal diffuse irradiance from hourly horizontal global radiation and assume that this correlation also is sufficiently valid for shorter time periods. A simple correlation of this type is given by Erbs et al. in Ref 5:

$$\frac{E_{sun}^{dh}}{E_{sun}^{gh}} = \begin{cases} 1.0 - 0.09K_c, \; K_c \le 0.22 \\ 0.9511 - 0.2604K_c + 4.388K_c^2 - 16.638K_c^3 + 12.336K_c^4, \; 0.22 < K_c \le 0.8 \\ 0.165, \; K_c > 0.8 \end{cases} \quad (8)$$

where E_{sun}^{dh} is the diffuse solar irradiance on a horizontal surface and E_{sun}^{gh} is the measured global (beam and diffuse) irradiance on the horizontal surface. The correlation in Eq. (8) is displayed in Figure 4

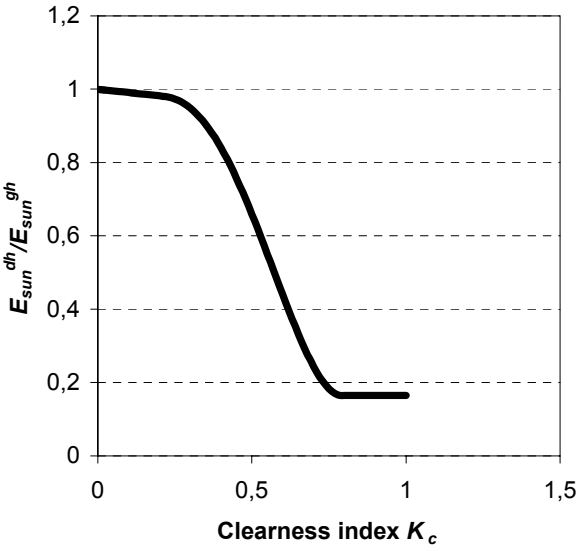

Figure 4 The correlation of Erbs et al. between the diffuse to global horizontal irradiation quotient, $E_{sun}^{dh}/E_{sun}^{gh}$, and the clearness index, K_c.

A more recent model for calculation of the hourly diffuse fraction has been presented by Skartveit et al. in Ref 7. In addition to the clearness index, the solar elevation and a statistical hour-to-hour variability index are also included as input parameters to this model. The variability index is included as a rough tool to statistically detect the presence of variable/inhomogeneous clouds. In Appendix B we briefly present the equations which we use from the model of Skartveit et al. In Figure 5 we show the diffuse fraction versus clearness index for three different solar elevations calculated with the model of Skartveit et al. In Figure 5 we have used a variability index of zero, corresponding to invariable cloud condition. In the model of Skarktveit et al. the diffuse fraction, as a function of clerarness index, assumes a minimum value for some $K_c = K_c^{crit} \le 1$. The reason for this is that Skarktveit et al. assume that clearness indices larger than K_c^{crit} arise from diffuse irradiance from clouds not obscuring the sun while the beam transmittance remains fixed for these large clearness indices.

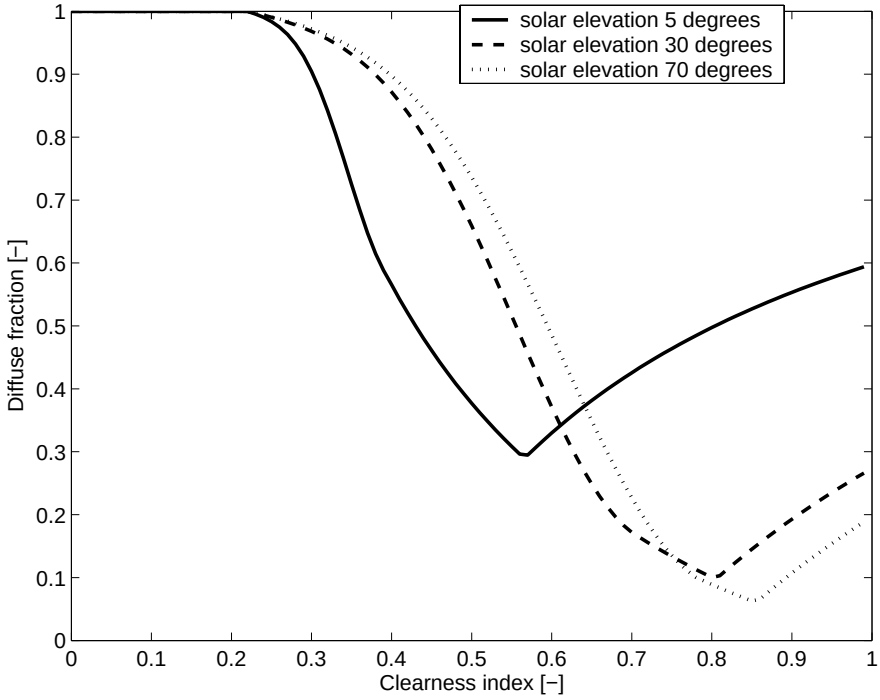

Figure 5 Diffuse horizontal fraction versus clearness index using the model of Skartveit et al. for invariable conditions.

We have performed a few tests of the performance of our semi-empirical model when using the diffuse fraction model of Erbs et al. and compared these to those obtained when using the model of Skartveit et al. The test cases (fitting the semi-empirical model to the radiance measurements presented in Section 6.1) show that the model of Skartveit et al. gives somewhat better results when used in combination with our semi-empirical model. We have therefore chosen to implement the model of Skartveit et al. as the default model for calculation of diffuse horizontal fraction.

The diffuse horizontal irradiance can be calculated using the model of Skartveit et al. (see Appendix B) and the horizontal beam irradiance, E_{sun}^{bh}, is then given by:

$$E_{sun}^{bh} = E_{sun}^{gh} - E_{sun}^{dh} \tag{9}$$

3.3 SHORT-WAVE AND LONG WAVE IRRADIANCE ON TILTED SURFACE

In the preceding subsection we showed how the diffuse and beam solar irradiation on a horizontal surface can be calculated from measured horizontal global (beam and diffuse) irradiance. We will now show how this can be used to calculate the global irradiance on a non-horizontal (tilted) surface.

Suppose that the flat surface element we consider has an outwards unit normal, $\hat{\mathbf{n}}_\mathbf{p}$, elevated an angle β_p from the horizontal and with an azimuth, $\alpha_p \in [0, 2\pi)$ ($[\bullet,\bullet)$ denotes the half open interval), from north (see Figure 6). By outwards unit normal to the surface we mean the unit normal pointing towards the air. This then defines the side of the surface which can receive radiation from the surroundings. The other side of the surface consists of the material

through which conduction heat transfer takes place and it cannot (in the model) receive radiation from the surrounding. However, we still allow for the surface unit normal to be directed towards the ground (negative β_p). This means that $\beta_p \in [-\pi/2, \pi/2]$. The position of the sun at a particular time of day at a specific geographical location is defined by the solar elevation, $\beta_s \in [-\pi/2, \pi/2]$, (from the horizontal) and the azimuth from north, $\alpha_p \in [0, 2\pi)$. We denote the unit vector directed towards the sun by $\hat{\mathbf{v}}_s$ (see Figure 6).

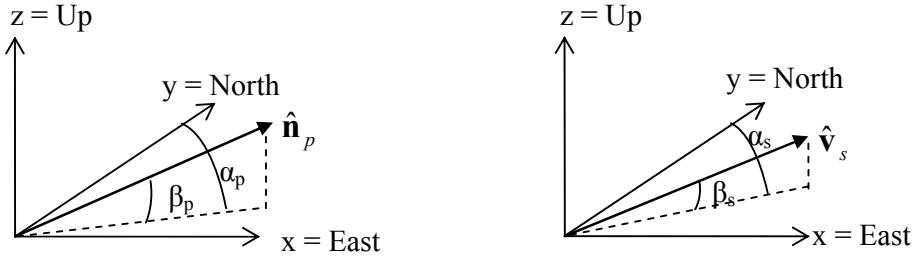

Figure 6 Definition of angles for the flat surface unit normal (left) and the solar position unit vector (right).

The surface unit normal vector and the unit sun vector, in the coordinate systems shown in Figure 6, can be expressed in their terms of respective angles as:

$$\hat{\mathbf{n}}_\mathbf{p} = (\sin\alpha_p \cos\beta_p, \cos\alpha_p \cos\beta_p, \sin\beta_p) \quad (10)$$

$$\hat{\mathbf{v}}_s = (\sin\alpha_s \cos\beta_s, \cos\alpha_s \cos\beta_s, \sin\beta_s) \quad (11)$$

Suppose that the horizontal beam irradiation, E_{sun}^{bh}, has been calculated using Eqs. (8) and (9). The solar beam irradiance on a surface perpendicular to the solar rays is then $E_{sun}^{bh}/\sin\beta_s$, provided that $0 < \beta_s \le \pi/2$ (i.e. the sun is above the assumed horizon). The solar beam irradiance on a surface with unit normal $\hat{\mathbf{n}}_\mathbf{p}$ at a point in time where the sun is at a position with sun vector $\hat{\mathbf{v}}_s$ is then given by:

$$E_{sun}^{bp} = \begin{cases} (E_{sun}^{bh}/\sin\beta_s)\cos\gamma = \hat{\mathbf{v}}_s \cdot \hat{\mathbf{v}}_p E_{sun}^{bh} / \sin\beta_s, & \cos\gamma > 0 \text{ and } \sin\beta_s > 0 \\ 0, & \cos\gamma < 0 \text{ or } \sin\beta_s < 0 \end{cases} \quad (12)$$

where γ is the angle between the vectors $\hat{\mathbf{n}}_\mathbf{p}$ and $\hat{\mathbf{v}}_s$. Furthermore we used the property of the scalar product that $\cos\gamma = \hat{\mathbf{v}}_s \cdot \hat{\mathbf{v}}_p$. A negative $\cos\gamma$ means that the surface is in shadow (self-shadowing).

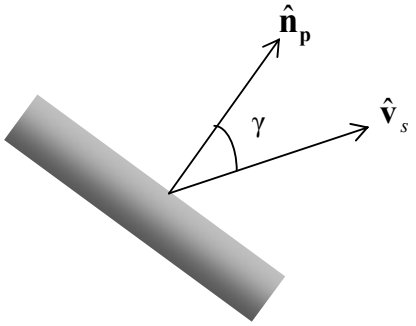

Figure 7 The angle, γ, between the surface normal and the sun vector.

Using the above equations we can calculate the solar beam irradiance on the tilted surface provided that we know the solar position (i.e. the elevation and azimuth) at all times. The solar position depends on the time (year, day of year and time of day) and also on the geographical position (latitude and longitude). We have downloaded a freeware Matlab™ program, `sunpos.m`, for calculation of the sun position from the internet, Ref 8. Input data to `sunpos.m` are year, day of year, time of day, latitude and longitude. We have compared the prediction of sun position using this code with the results from other codes and models and the agreement is very good.

Now we also need to calculate the diffuse irradiation on the tilted surface. What we need to take into account here is that a tilted surface can only "see" a fraction of the sky hemisphere and also that it can "see" a fraction of the ground, which we here consider as flat. The solid angle fraction of the sky hemisphere which can be viewed from the tilted surface is the view factor (see for instance Ref 9 for more on view factors) for the sky hemisphere to tilted surface heat transfer. This view factor, F_{sky}, is given by (see Figure 8):

$$F_{sky} = \frac{\int_0^{\pi/2+\beta_p}\int_0^{\pi} \sin\theta d\theta d\varphi}{2\pi} = \frac{\pi(1-\cos(\pi/2+\beta_p))}{2\pi} = \frac{1}{2}(1+\sin\beta_p) \qquad (13)$$

where $\beta_p \in [-\pi/2, \pi/2]$ as mentioned earlier. In the same way, the solid angle fraction of the ground (assumed flat and infinite), which can be viewed from the tilted surface is the view factor for the ground to tilted surface heat transfer. This view factor, F_{ground}, is given by (see Figure 8):

$$F_{ground} = \frac{\int_0^{\pi/2-\beta_p}\int_0^{\pi} \sin\theta d\theta d\varphi}{2\pi} = \frac{\pi(1-\cos(\pi/2-\beta_p))}{2\pi} = \frac{1}{2}(1-\sin\beta_p) \qquad (14)$$

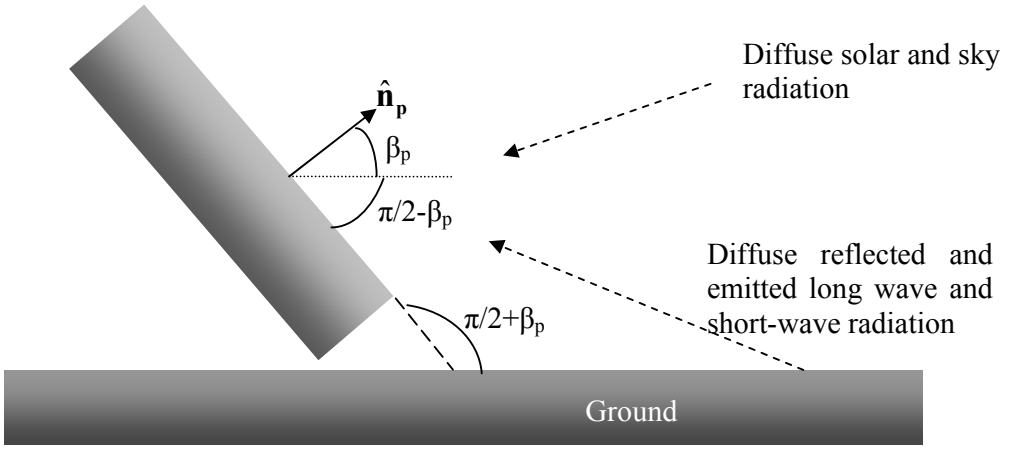

Figure 8 Angles for calculation of view factors for a tilted surface.

We can now use the view factors to calculate the diffuse irradiance on the tilted surface, provided that we know the horizontal diffuse solar irradiance, E_{sun}^{dh}, the horizontal (diffuse and long wave) sky irradiation, E_{sky}^{dh} and also the horizontal shortwave radiation reflected from the ground, E_{gshort}^{dh}, and the horizontal long wave ground radiation, E_{glong}^{dh} (see Figure 9). Here we will assume that the radiation from the ground (i.e. reflected and emitted) is diffuse.

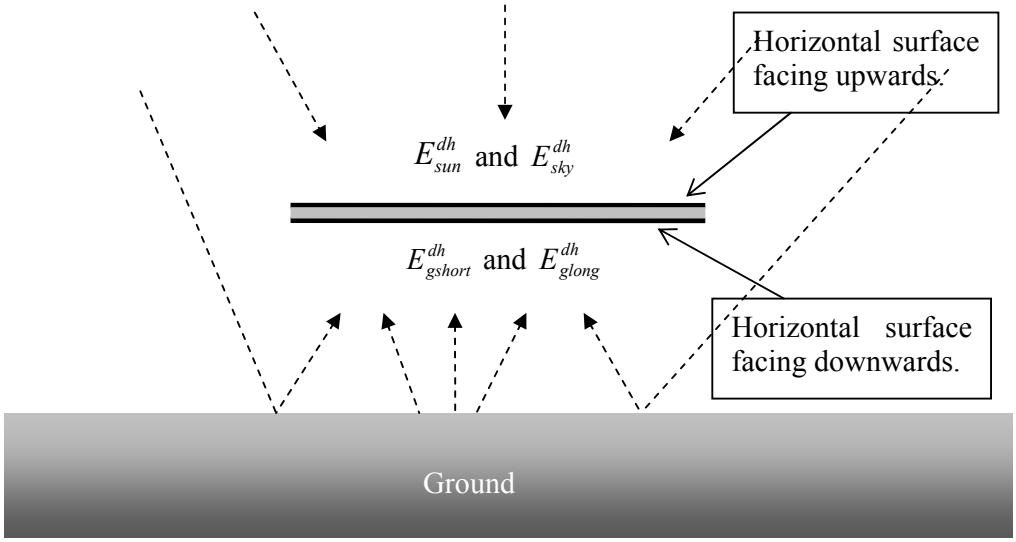

Figure 9 Components of diffuse radiation on horizontal surfaces facing upwards and downwards respectively.

The horizontal diffuse solar irradiation, E_{sun}^{dh}, can be calculated from the measured horizontal global irradiation using the model of Skartveit et al. The other diffuse horizontal irradiations, E_{sky}^{dh}, E_{gshort}^{dh} and E_{glong}^{dh}, can be considered to be measured directly by the weather station since it has sensors which measures long wave and shortwave irradiation on pairs of horizontal plates like in the schematic Figure 9 . In Section 2.2 where we considered horizontal surfaces,

we identified E_{sky}^{gh} with E_{sky} and in that case E_{gshort}^{dh} and E_{glong}^{dh} were zero. We can now calculate the total diffuse short-wave irradiance, E_{short}^{dp}, and long wave irradiance, E_{long}^{dp}:

$$E_{short}^{dp} = F_{sky}E_{sun}^{dh} + F_{ground}E_{gshort}^{dh} \tag{15}$$

$$E_{long}^{dp} = F_{sky}E_{sky}^{dh} + F_{ground}E_{glong}^{dh} \tag{16}$$

where the view factors F_{sky} and F_{ground} are given by Eqs. (13) and (14) respectively. However, in Eq. (15) we assume that the diffuse solar radiation is uniformly distributed over the sky dome. In reality the diffuse solar sky radiance is anisotropic due to (for instance) forward scattering in the form of circumsolar radiation and increased scattering from longer pathlengths near the horizon, horizon brightening. Klucher, Ref 10, has suggested two empirical factors, M_1 and M_2, to account for circumsolar radiation and horizon brightening. In our case this amounts to replacing Eq. (15) with:

$$E_{short}^{dp} = F_{sky}M_1M_2E_{sun}^{dh} + F_{ground}E_{gshort}^{dh} \tag{17}$$

where

$$M_1 = 1 + \left[1 - (E_{sun}^{dh}/E_{sun}^{gh})^2\right]\sin^3(\pi/4 - \theta_p/2) \tag{18}$$

$$M_2 = 1 + \left[1 - (E_{sun}^{dh}/E_{sun}^{gh})^2\right]\cos^2(\gamma)\cos^3\theta_s \tag{19}$$

As was mentioned in Section 3.1 we presently assume that the long wave sky irradiance is isotropic over the sky dome. Anisotropic long wave sky irradiance could be considered in further developments of the model.

We can now put it all together and calculate the global long wave and short wave irradiance on the tilted (non-horizontal) surface. We denote these irradiances by E_{long}^{gp} and E_{short}^{gp}, respectively. The result is:

$$E_{short}^{gp} = E_{short}^{dp} + E_{sun}^{bp} \tag{20}$$

$$E_{longt}^{gp} = E_{long}^{dp} \tag{21}$$

where the short-wave and long wave diffuse irradiations (E_{short}^{dp} and E_{long}^{dp}) are given by Eqs. (17) and (16), and the solar beam irradiation (E_{sun}^{bp}) is given by Eq. (12).

3.4 THE SEMI-EMPIRICAL MODEL AND NON-HORIZONTAL SURFACES

Suppose that the global short-wave and long wave irradiances, E_{short}^{gp} and E_{long}^{gp} in Eqs. (20) and (21), have been calculated from the measured horizontal irradiances as described in Subsection 3.3. All we need to do then is to identify E_{sun} in Eq. (2) in Subsection 2.1 with the

calculated E_{short}^{gp} and also in the same way identify E_{sky} in Eq. (2) with E_{long}^{gp}. When doing this identification the semi-empirical model presented in Subsection 2.1 and all equations therein remain valid. This completes our treatment of non-horizontal surfaces and in Section 6 we will show results from applying the semi-empirical model to a couple of examples of tilted surfaces.

4 PRECIPITATION AND LATENT HEAT

In the semi-empirical model presented in Subsection 2.1, and in Ref 1, we did not account for precipitation on the surface and neither did we account for evaporation and condensation of water in the heat balance fluxes. Precipitation can be in the form of snow, rain, sleet or hail. However, for simplicity we will only consider precipitation in the liquid phase, i.e. rain. The process of condensation of water vapor on the surface give energy to the surface and evaporation takes energy. Evaporation and condensation is in heat transfer referred to as latent heat. Sometimes the transpiration of vegetation is also included when considering latent heat. In general, latent heat depends on several parameters in a complicated manner. It depends on for instance turbulent transport (as in convection), on the material and the moisture content in the material. Furthermore, when considering latent heat and vegetation, the latent heat transfer depends on the vegetation type.

Thermal effects of precipitation and, in particular, latent heat are very difficult to model correctly. Furthermore, even the simple models we consider for precipitation and latent heat will have to be approximated further in order to retain the relative simplicity of the semi-empirical model. The precipitation and latent heat additions to the semi-empirical model which we present here are therefore at present optional models in our implementation of the semi-empirical model and they will remain so until a more thorough evaluation and validation has been performed.

The precipitation heat flux, Φ_{perc}, and the latent heat flux, Φ_{lat}, can be included in Eq. (1) as :

$$\frac{dT_s}{dt} = \frac{k_1}{\rho c d}\left[\Phi_{sun} + \Phi_{sky} + \Phi_{emiss} + \Phi_{conv} + \Phi_{perc} + \Phi_{lat}\right] + \frac{k_2}{P_e}(T_s - T_0) \qquad (22)$$

4.1 PRECIPITATION

We will include a very simple treatment of precipitation in the semi-empirical model. We assume that the precipitation is in the form of vertically falling raindrops. A simple caliometric argument then gives that the rain heat flux, Φ_{perc}, on a flat surface, with surface normal elevated an angle β_p from the horizontal, can be expressed as:

$$\Phi_{perc} = (T_w - T_s)\rho_w C_w \dot{p} \max(\sin\beta_p, 0) \qquad (23)$$

where $T_W \approx T_a$ is the water temperature in raindrops which we assume to be equal to air temperature, ρ_w the water density, C_w the volume heat capacity of water and $\dot{p}$ is the precipitation rate (dimension [length/time]). We treat the rain heat flux analogously to the convection heat flux when passing from Eq. (1) to Eq. (3) in Subsection 2.1 (see Appendix A for details) and this simply results in replacing Eq. (3) with

$$L(t) \approx \int_{t_0}^{t} e^{-B_0(t-s)} \sum_{i=1}^{5} A_i P_i(s) ds + D + \sum_{i=1}^{2} C_i P_i \,, \tag{24}$$

where $P_5 = T_a \dot{p}$ and A_5 is a new free parameter which can be determine through linear regression.

4.2 LATENT HEAT

In this subsection we will present a relatively crude treatment of latent heat which we have implemented in the semi-empirical model, primarily for continued evaluation and development. A relative simple model for the soil latent heat transfer flux, Φ_L is (Ref 11):

$$\Phi_L = r\tilde{h}(v)(H_r e(T_a) - H_s e(T_s)) \,, \tag{25}$$

where H_r is the relative humidity in the air, H_s is the relative humidity of the air which is in contact with the surface, $e(T_a)$ is the saturation pressure (Pa) at air temperature, $e(T_s)$ is the saturation pressure (Pa) at the surface temperature, $\tilde{h}(v)$ is a convection factor (Wm^{-2}/K) and finally r is a conversion factor (K/Pa). In Section 2.1 we chose a convection factor of the form $h(v) = a_1 + a_2 v^{0.7}$ where a_1 and a_2 are treated as unknown constants for free and forced convection to be determined (in combinations with other parameters) in the regression. However, in order to keep the regression free from constraints (to treat dependent variables), or alternatively to keep the number of free parameters to a minimum, we choose to specify the convection factor in the latent heat flux to be $\tilde{h}(v) = a(5.6 + 2.8v)$, Ref 11, where a is the single unknown constant.

Many expressions for the saturation pressure can be found in the literature. A simple semi-empirical formula for the saturation pressure of vapor (above liquid water) is given by (Ref 12):

$$e(T) = 611.2 e^{17.67(T-273.15)/(T-29.65)} \text{ (Pa)}, \tag{26}$$

where T is the temperature in Kelvin. In Figure 10 we show the saturation vapor pressure versus temperature according to Eq. (26).

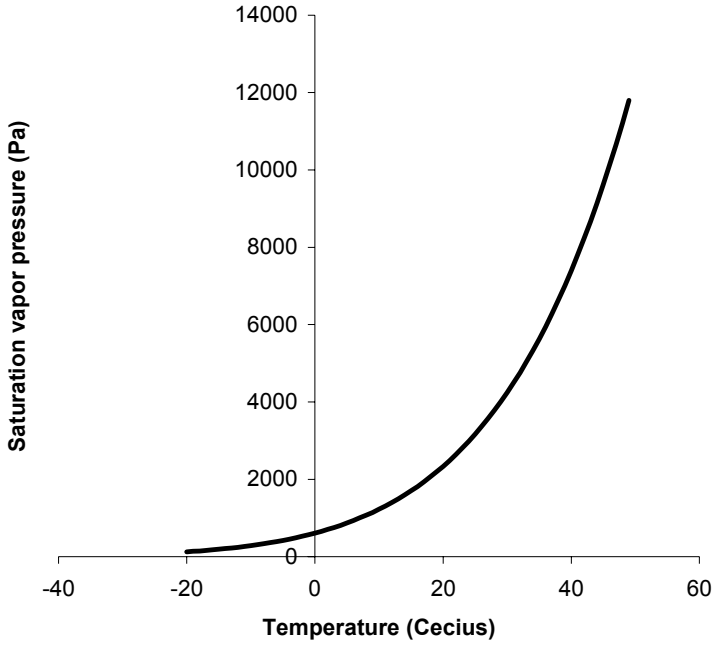

Figure 10 Saturation vapor pressure versus temperature.

Although Eq. (25) is only a simple formulation of latent heat we still have to introduce further approximations to incorporate it easily in our semi-empirical model. The relatively severe non-linearity of the saturation pressure, also at ordinary ground temperatures, makes it difficult to incorporate directly in our linear model. We have therefore implemented a simple iterative (the semi-empirical algorithm is run two times) treatment of latent heat for evaluation purposes in our semi-empirical model. This iterative process consists of the following steps:

1. Calculate estimates of the radiance, L_0, for all times using the semi-empirical model (as described in Sections 2 and 3) without accounting for latent heat transfer. From the radiance L_0 we approximately calculate the corresponding apparent (blackbody) temperature (see Figure 17 in Appendix A) of the surface, T_s^{a0}.
2. Use the calculated apparent temperatures as estimates of the surface temperature in the latent heat flux in Eq. (25) (and (26)) and perform a new calculation (fit and/or prediction) of the radiance.

In step 1 we presently assume that the considered wavelength band is 8-12 μm but this could easily be generalized in the implementation. In step 2 above we replace Eq. (24) with

$$L(t) \approx \int_{t_0}^{t} e^{-B_0(t-s)} \sum_{i=1}^{6} A_i P_i(s) ds + \sum_{i=1}^{2} C_i P_i + D, \qquad (27)$$

where A_6 is a new free parameter and we have implemented two different forms of the quantity P_6 for further (future) evaluation. The first form of P_6 amounts to simply replacing

the actual surface temperature, T_s , in Eq. (25) with the calculated apparent temperature, T_s^{a0}, so that

$$P_6 = \widetilde{h}(v)[H_r e(T_a) - H_s e(T_s^{a0})] \tag{28}$$

The other proposed form of P_6 is based on Taylor expanding $e(T_s)$ in Eq. (25) about T_s^{a0} up to linear terms in T_s . In this case the treatment in step 2 above involves analogous assumptions to the treatment of the convection heat flux when passing from Eq. (1) to Eq. (3) in Subsection 2.1 (see Appendix A for details) and the form of P_6 becomes:

$$P_6 = \widetilde{h}(v)[H_r e(T_a) - H_s e(T_s^{a0})(1 - 4302.6 T_s^{a0} / (T_s^{a0} - 29.65)^2)] \tag{29}$$

We could in principle repeat Steps 1 and 2 and do more iterations to obtain better estimates of the surface temperature (i.e. a more accurate T_s^{a0}). In the implementation of these equations the user is presently allowed to provide a value on H_s, $0 \le H_s \le 1$, as input. A value $H_s = 1$ means that the air in contact with the surface element has 100% relative humidity, and could be a reasonable assumption when applying the model to ground surfaces such as for instance moist soil.

5 IMPLEMENTED MODEL IN BRIEF

We have implemented the semi-empirical model as presented in previous sections in a Matlab code which we presently call SEMSIM1.0. The code is presently very much a research tool which is still being developed. Therefore, we only give a very brief overview of the code and the input data. However, we have tried to make the program reasonably general and easy to use even though it presently lacks a Graphical User Interface (GUI). The code presently consists of six Matlab functions:

`semsim1main.m`: The program main which is executed in a run.
`semsimparamfit.m`: Performs fitting of parameters.
`semsimprediction.m`: Performs predictions using fitted parameters.
`irradtilt.m`: Performs calculation of irradiances on tilted surface as in Section 3.3.
`sunpos.m`: Calculation of sun position.
`day2jd.m`: Calculation of Julian day (day of year) for use in calculation of sun position.

Defining paths and names of output catalogues, input weather files and measured radiance data files as well as specifying surface position, model options and the type of calculation are made in an input definition file in Microsoft Excel format with the name `input.xls`. An example of an input definition file is given in Appendix C. Weather data and measured data are also provided in files in Microsoft Excel format. We will not specify the input formats for these files here but examples of the first few lines of a weather data file and a radiance measurement file are given in Appendix C. Of importance is that times are given in a format with year and date and that the time provided is in UTC (Universal time).

As was mentioned in Section 4, precipitation and latent heat are presently optional additions when running the code.

6 RESULTS AND EXAMPLES

In this section we present some results from applying the semi-empirical model presented in the previous sections when applied to non-horizontal surfaces.

6.1 MEAUREMENTS ON TILTED PANELS

In order to test our "ansatz" for treating non-horizontal surfaces in the semi-empirical model we need measurements of radiance from some tilted surfaces over some periods of time. We also need measured weather data for the same time period and preferably, for application of our model, the measurements of weather data should have begun prior (how much depends on the thermal inertia) to the radiance measurements.

We have chosen to use the measurements of two tilted panels with different types of coatings that were performed by the Swedish Defence Research agency during 8-9 April 2003. The two panels have quite different surface emissivities, one is close to unity and the other is approximately 0.5. We refer to the panel with emissivity close to unity as the *paint panel* and the panel with low emissive coating as the *foil panel*. These measurements were performed for the purpose of validating commercial IR signature programs and the measurements are presented in Ref 13. The radiance measurements, in MWIR and LWIR using IR (Thermovision) cameras, were performed during a full 24-hour period and measurements of weather data begun almost 24 hours before the radiance measurements. During the 8th the sky was clear and the weather sunny. The 9th the sky was cloudy and at about 13:00 it started to rain mixed with snow. Soon after that the experiment was stopped. Radiance data and weather data were collected with a time interval of about one minute in between individual measurements. The tilted panels consist of different layers that form a flat surface of 1 x 1.2 m^2. A cross-section of the panels and a photograph of the panels at the measurement site is shown in Figure 11 (the images are from Ref 13).

Figure 11 Cross section of the panels and a photo of the two panels on stands (paint panel to the left).

After the measurements were completed, calibrated radiance data were calculated and the radiance was corrected for atmospheric transmission losses, which gave the radiance at the panel surfaces. From these data the mean radiance over the panel surface was calculated and it is these data we will use in the next subsection. Some position data for the panel measurements are displayed in Table 2. For more information see Ref 13.

Table 2 Position data for the panel measurements

Geographical Position:	**Latitude**	**Longitude**
	N 58º 23,505	E15º 34,537
Surface normal direction:	**elevation β_p**	**azimuth α_p**
	30°	256°

6.2 RESULTS AND ANALYSIS OF TILTED PANELS

The geometry and material composition of the panels make the heat transfer problem essentially one-dimensional and the fact that the panels have a layer of insulation underneath the coatings and aluminium layers makes the panels thermally "thick" so that heat fluxes on the back side of the panel essentially do not affect the front side temperature. Also, the weather data measurements were performed in close proximity (a few meters) to the panels. These factors should make the panels well suited as a test case for applying the semi-empirical model on non-horizontal surfaces.

In order to assess if the methods and equations presented in Section 3 improves the accuracy of the semi-empirical model for tilted surfaces, we have performed some comparative tests. We have compared results obtained by not including the non-horizontal surface corrections with results obtained by including all, or only some, of the further developments. The comparisons show that by including the methods in Section 3 step-by-step we steadily improve the accuracy when curve-fitting the model to the panel measurements. For instance, the root mean square (RMS) error is reduced from 1.887 to 0.387 W/(m^{2}sr) for the paint panel in LWIR and for the foil panel in LWIR it is reduced from 1.208 to 0.541 W/(m^{2}sr) when including all corrections presented in Section 3. In Figure 12 we show a comparison of results obtained by curve-fitting the semi-empirical model, with and without corrections to treat a non-horizontal surface, to measurements on the paint panel in LWIR.

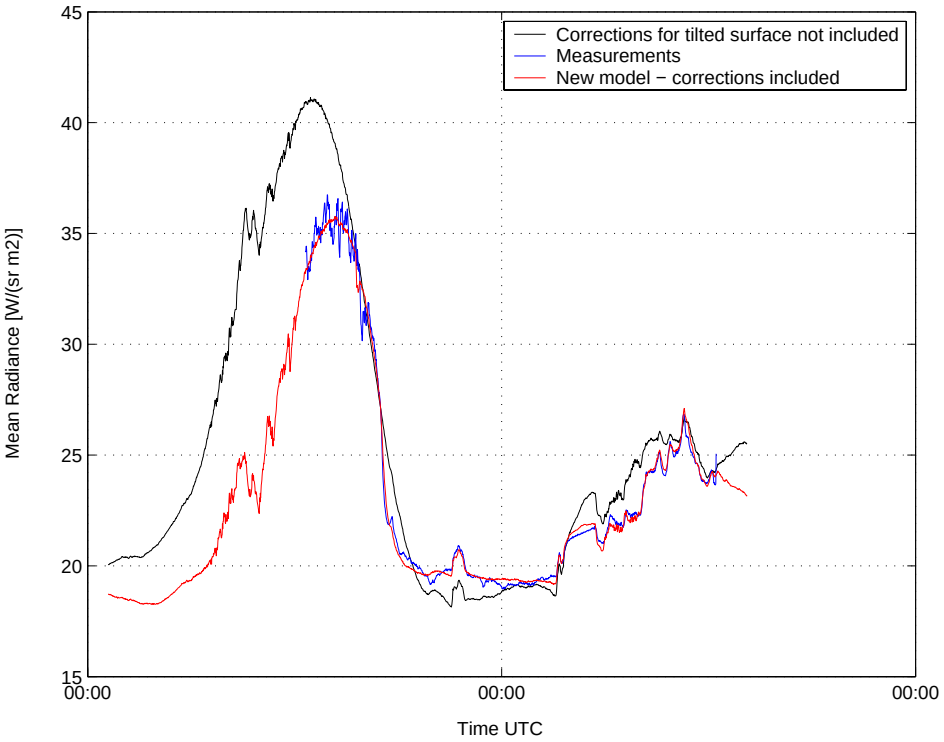

Figure 12 Comparison of results obtained by curve-fitting the semi-empirical model, with and without corrections to treat a non-horizontal surfaces, to measurements on the paint panel in LWIR.

In Figure 13 and Figure 14 we show the results obtained by curve-fitting the new semi-empirical model to radiance measurements on the paint and foil panels, respectively. Included in these plots are also the residuals for the fits. The agreement between the curve-fitted semi-empirical model and the measured data can be considered to be very good for these test cases.

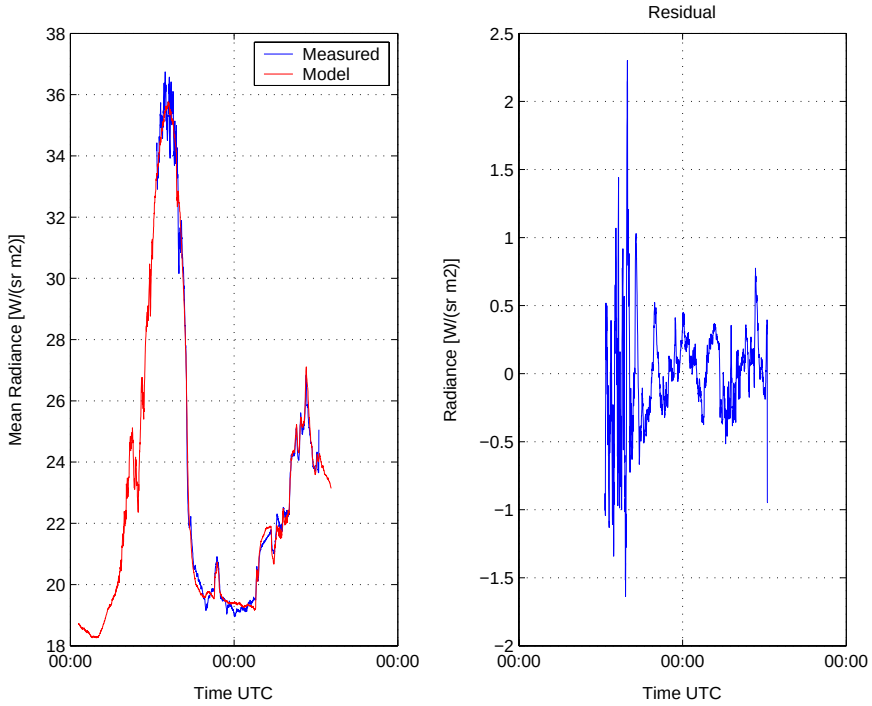

Figure 13 Result obtained by curve-fitting the new semi-empirical model to radiance measurements on the paint panel.

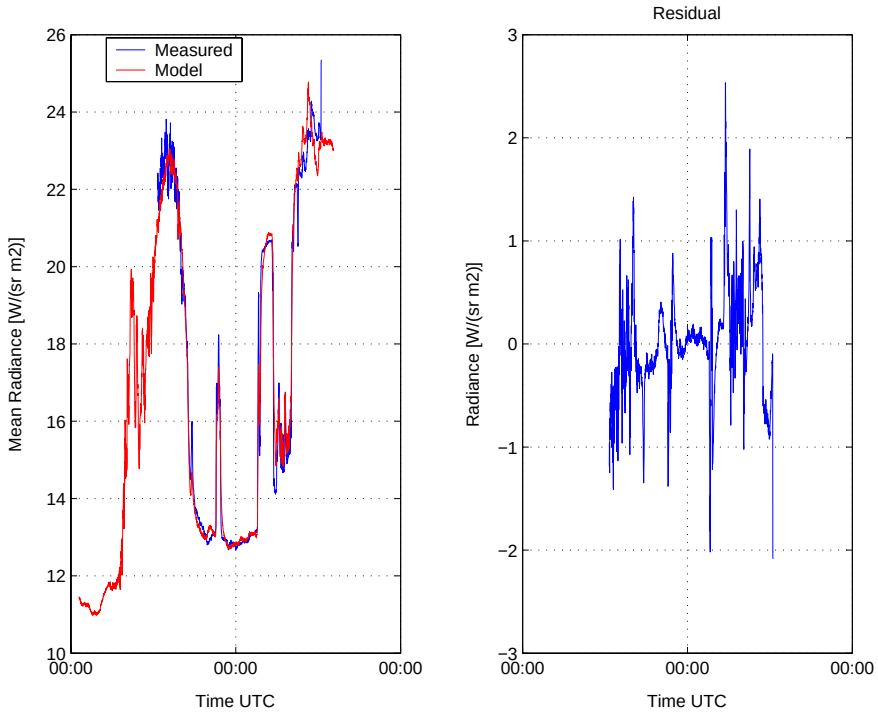

Figure 14 Result obtained by curve-fitting the new semi-empirical model to radiance measurements on the foil panel.

We have performed one more test to evaluate the (qualitative) performance of the improved semi-empirical model. Using the model parameters determined in the regression presented above we have calculated the predicted radiance from the two panels for the cases when the

panels have been positioned so that their surface normals have an elevation of 30° and azimuths 0° (North), 90° (East) and 180° (South). This simply means that the panels have been rotated in the azimuthal direction. We have used the same weather data as before in these calculations. The results of these calculations are shown in Figure 15 and Figure 16. Although we do not have any measurements to compare these predictions with, the calculations show that the model, at least qualitatively, behaves as expected for these cases.

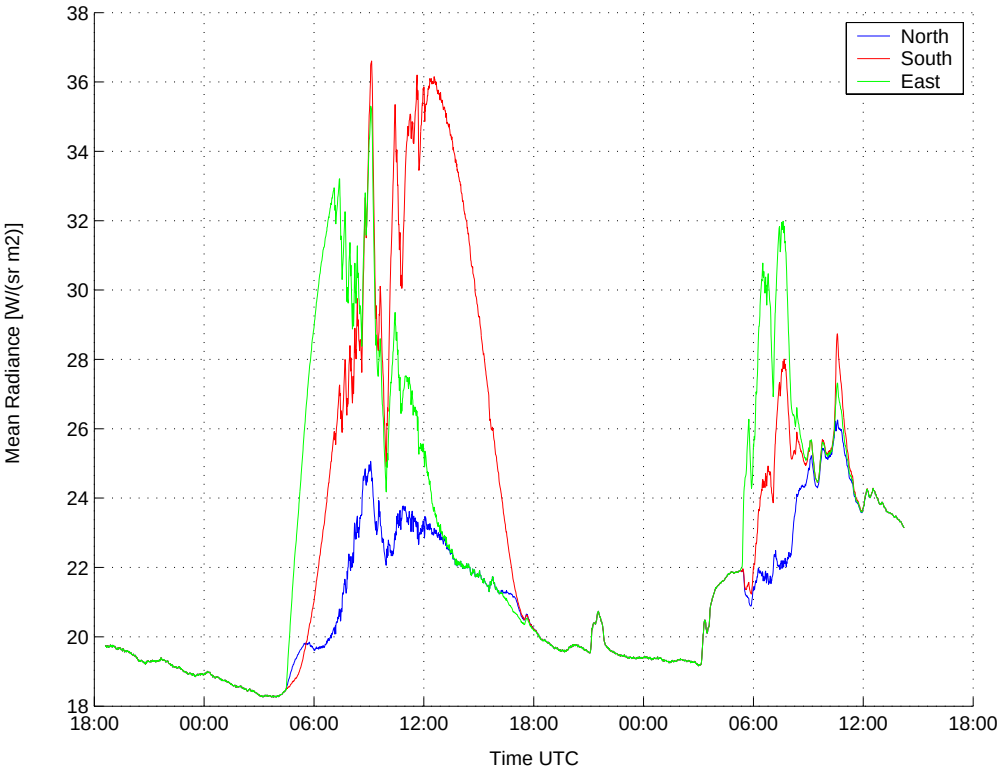

Figure 15 Pridicted radiance from paint panel with surface normal elevation 30° and azimuths 0° (North), 90° (East) and 180° (South).

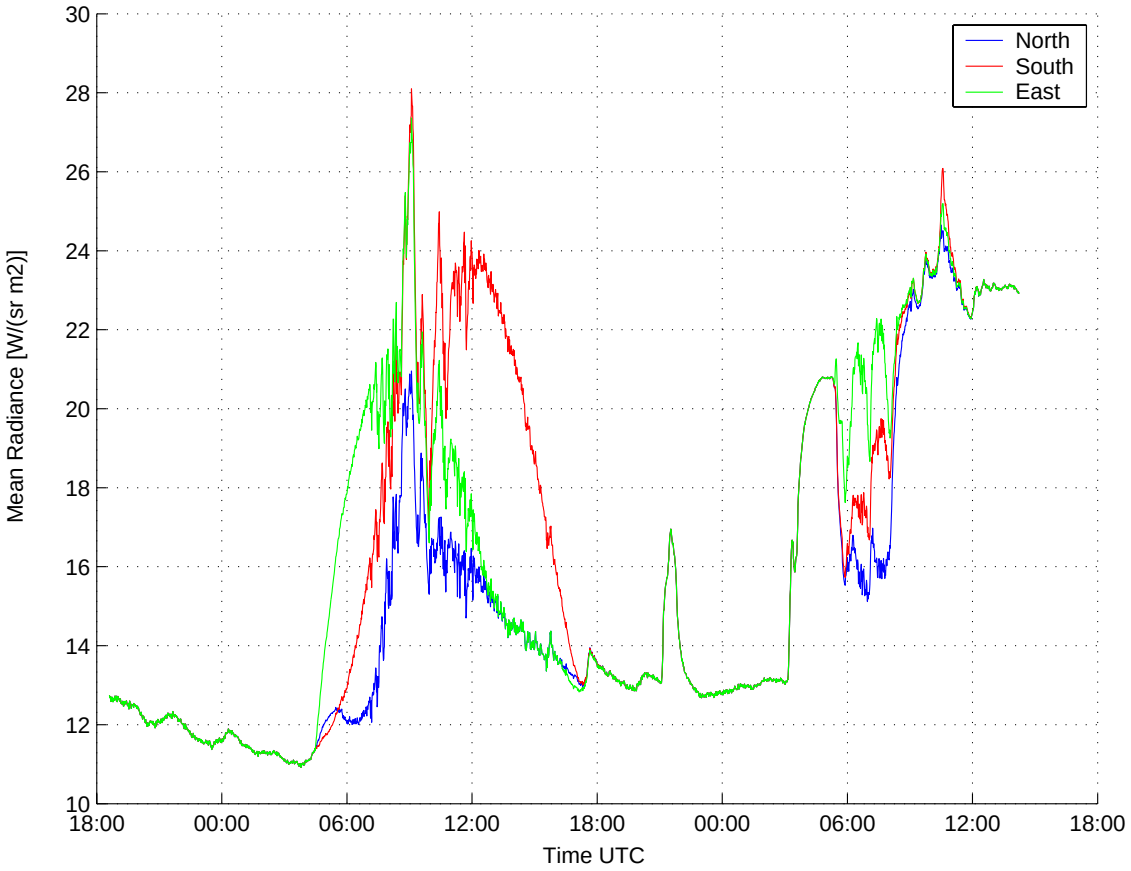

Figure 16 Pridicted radiance from the foil panel with surface normal elevation 30° and azimuths 0° (North), 90° (East) and 180° (South).

6.3 REMARKS ON LATENT HEAT AND PRECIPITATION

At present we have not made a proper evaluation of the proposed models for latent heat and precipitation which were presented in Section 4. However, during the measurements on the two panels, a mixture of rain and snow fell on the ground and the panels towards the very end of the measurements (i.e. during a very short period of time). By including the proposed precipitation heat flux model in the curve-fitting to the panel data, the result are essentially unchanged for the paint panel while the result improve slightly (RMS error decreases from 0.541 to 0.528) for the foil panel. There can also be mechanisms associated with precipitation which we presently do not account for in the semi-empirical model. An example of such a mechanism is that the surface emissivity (and reflectivity) that can change when the surface becomes wet. In order to assess the validity and usefulness of the precipitation heat flux model, a more extensive evaluation has to be performed.

As far as the proposed model for latent heat flux is concerned, we have so far only made a single test on a grass background element (element number 3 in LWIR during the May measurements in Ref 1). The inclusion of the proposed model for latent heat in the semi-empirical model results in only a very small decrease in the RMS error for this case. No conclusions can be drawn from this test and further evaluation and possibly further development is needed to assess latent heat in the semi-empirical model.

7 CONCLUSIONS AND FURTHER DEVELOPMENT

In this note we have presented further developments that have been made on a previously presented semi-empirical model for calculation of thermal IR signatures from background elements. An improved modeling of non-horizontal surfaces has been included in the semi-empirical model. The model has been tested by curve-fitting to time histories of measured LWIR radiance from two flat, tilted panels. The curve-fitting gives a good agreement between model and measurements for both panels during the entire time period for which we have measurements. For the purpose of future evaluation we also present proposals on how simple models for latent heat and precipitation can be included in the semi-empirical model.

The promising results obtained with the semi-empirical model strengthen our belief that this model could be of use, as a complement to other tools (for instance commercial programs), for thermal IR signature prediction applications. For cases where some measured surface radiance and weather data are available, but reliable data on thermophysical material parameters is lacking, the semi-empirical model provides a tool for predicting thermal IR signatures when other tools cannot be used. The semi-empirical model is also a relatively simple and easy-to-use tool for evaluating the effects of different weather conditions on the IR signature from simple objects or new material compositions. The semi-empirical model could also be used as a tool in the modeling of time histories of textural and statistical features of IR images. Furthermore, under some conditions, the semi-empirical model is likely to able to approximately predict the effects of temporal variations in the environmental conditions (for instance changing cloudiness), which are either quite difficult or time consuming to predict with the commercial signature prediction software currently used at FOI.

There are numerous directions in which the semi-empirical model could be developed further. Of great importance would be to further evaluate and validate the model for IR signature prediction purposes. The models for latent heat and precipitation which we have presented in this note should be evaluated further and possibly also developed further. Other examples and suggestions of further developments are:

- Explicitly accounting for multi-layer conduction heat transfer in the model. Non-linear regression could also be considered.
- Use weather data where the diffuse and global sun irradiances are measured separately. This would require some additional equipment on the weather station which is currently used. This would remove some uncertainties in the model.
- Use the model for prediction of statistical and textural features of IR signatures.
- Improving the in-band and radiometric capabilities of the model to improve modeling of different wavelength bands in the infrared. Simple models for treating anisotropic reflectance could perhaps also be considered.
- Examine the prospect of using the semi-empirical model for determining unknown thermophysical parameters (an inverse problem). In the process of curve-fitting the model, combinations of thermophysical parameters are determined. It would be of interest to investigate to what extent individual thermophysical parameters can be determined and then also to assess how accurate these calculated parameters are.
- Improved modeling of the surrounding terrain. In the present model the surrounding terrain is essentially assumed to be flat and homogeneous. This, in general, require a

full 3D modeling of the surrounding and this is a huge task in itself and therefore the following could be a more reasonable approach in some cases:

- The semi-empirical model could be used to calculate surface temperatures or the radiance from different surface elements. These results could then possibly be used as input to a (commercial) 3D simulation software.

8 REFERENCES

Ref 1 P. Hermansson, Sten Nyberg and Claes Nelsson, ”IR background modelling – progress report”, FOI-R--0529--SE, 2002.

Ref 2 M. Hansson, “Analys av temperaturdifferens mellan luft och bakgrund – statisstisk modellering”, FOI-R--0853--SE, 2003.

Ref 3 J. W. Deardorff, ” Efficient prediction of ground surface temperature and moisture , with an inclusion of a layer of vegetation”, J. Geophys. Res. **83**(C4), pp 1889-1904, 1978.

Ref 4 A. Mahmoodi, A. Nabavi and M. N. Fesharaki, “Infrared image synthesis of desert backgrounds based on semi-empirical thermal models”, Opt. Eng. 40(2), pp 227-236, 2001.

Ref 5 D. G. Erbs, S. A. Klein and J. A. Duffie, “Estimation of the diffuse radiation fraction for hourly, daily and monthly-averaged global radiation”, Solar Energy 28, pp 293-302, 1982.

Ref 6 http://solardat.uoregon.edu/download/DataBk /XCorrelationsBetweenDiffuseAndGlobalIrradiance.pdf

Ref 7 A. Skartveit, J. A. Olseth and M. E. Tuft, ”An hourly diffuse fraction model with correction for variability and surface albedo”, Solar Energy 63, pp 173-183, 1998.

Ref 8 Matlab code for calculation of sun position downloaded from: http://www.igf.fuw.edu.pl/meteo/stacja/kody.htm

Ref 9 A. Bejan, “Heat Transfer”, John Wiley & Sons Inc., 1993.

Ref 10 T. M. Klucher, ”Evaluation of models to predict insolation on tilted surfaces”, Solar Energy, 23, pp 111-144, 1979.

Ref 11 A. B. Kahle, ”A simple thermal model of the earth’s surface for geologic mapping by remote sensing”, J. Geophys. Res. vol 82, no 11, pp 1673-1680, 1977.

Ref 12 D. Bolton, ”The calculation of equivalent potential temperature”, Monthly Weather Review, 108, pp 1046-1053, 1980.

Ref 13 P. Hermansson, A. Hjelm, R. Lindell, C. Nelsson, A. Persson, S. Sjökvist and T. Winzell, ”Benchmarking and validation of IR signature programs: SensorVision, CameoSim and RadThermIR, FOI-R--0952--SE, 2003.

APPENDIX A DERIVATION OF MODEL ALGORITHM

In this appendix we present the assumptions and steps involved in the derivation of the incremental algorithm for the semi-empirical model, Eqs. (4) and (5), in a bit more detail.

Begin by considering a Force-Restore type equation:

$$\frac{dT_s}{dt} = \frac{k_1}{\rho c d}\left[\alpha_{sun} E_{sun} + \varepsilon E_{sky} - \varepsilon\sigma T_s^{\,4} - h(v)(T_s - T_a)\right] - \frac{k_2}{P_e}(T_s - T_0) \tag{A.1}$$

We assume a convection factor of the form $h(v) = a_1 + a_2 v^{0.7}$ and we linearize $T_s^{\,4}$ term so that $\varepsilon\sigma T_s^{\,4} \approx b_1 + b_2 T_s$, which is reasonably accurate for ordinary ground temperatures. Eq. (A.1) can then be put in the form:

$$\frac{dT_s}{dt} = -\left[\frac{k_1}{\rho c d}\left(h(v) + b_2\right) + \frac{k_2}{P_e}\right] T_s + \frac{k_1}{\rho c d}\left[\alpha_{sun} E_{sun} + \varepsilon E_{sky} + h(v) T_a - b_1\right] + \frac{k_2}{P_e} T_0 \tag{A.2}$$

Eq. (A.2) is a linear first order ordinary differential equation of the type:

$$\frac{dT_s}{dt} = -B(t) T_s + \sum_{i=1}^{N} A_i P_i(t) + D \tag{A.3}$$

where in Eq. (A.2) $N = 4$ and

$$\begin{aligned}
B(t) &= \frac{k_1}{\rho c d}\left(h(v) + b_2\right) + \frac{k_2}{P_e} = B_0(\gamma_1 + \gamma_2 v^{0.7}) \\
A_1 &= \frac{k_1}{\rho c d}\alpha_{sun} & P_1 &= E_{sun} \\
A_2 &= \frac{k_1}{\rho c d}\varepsilon & P_2 &= E_{sky} \\
A_3 &= \frac{k_1}{\rho c d} a_1 & P_3 &= T_a \\
A_4 &= \frac{k_1}{\rho c d} a_2 & P_4 &= T_a v^{0.7} \\
D &= \frac{k_2}{P_e} T_0 - \frac{k_1}{\rho c d} b_1
\end{aligned} \tag{A.4}$$

The problem we like to solve is therefore

$$\begin{cases} \dfrac{dT_s}{dt} = -B(t)T_s + \sum_{i=1}^{N} A_i P_i + D \\ T_s(t_0) = C \end{cases} \tag{A.5}$$

where $T_s(t_0) = C$ is some initial condition.

We make a change of variables (remember that $B(t)$ and B_0 are greater than zero).

$$\tau = \frac{1}{B_0}\int_{t_0}^{t} B(t)dt = \int_{t_0}^{t} (\gamma_1 + \gamma_2 v^{0.7})dt\,, \tag{A.6}$$

Eq. (A.5) becomes

$$\frac{dT_s}{d\tau} = -B_0 T_s + \sum_{i=1}^{N} A_i \frac{P_i}{\gamma_1 + \gamma_2 v^{0.7}} + \frac{D}{\gamma_1 + \gamma_2 v^{0.7}} \tag{A.7}$$

Eq. (A.7) can be solved by standard methods and the solution is:

$$T_s(\tau) = \int_0^{\tau} e^{-B_0(\tau - s)} \left[\sum_{i=1}^{N} A_i \frac{P_i}{\gamma_1 + \gamma_2 v^{0.7}} + \frac{D}{\gamma_1 + \gamma_2 v^{0.7}} \right] ds + Ce^{-B_0\tau} \tag{A.8}$$

Since the time constant $B_0 > 0$, the last term in (A.8) can be made arbitrarily small by considering large enough times (τ is a strictly monotonic function of the time, *t*) and the solution therefore becomes independent of the initial condition for large enough times. Eq. (A.8) could be used as the basic expression which we fit to measurements but it doesn't give rise to a linear least square problem. We therefore reconsider Eq. (A.6) which can be written:

$$\tau = \int_{t_0}^{t} (\gamma_1 + \gamma_2 v^{0.7})dt = \gamma_1 (t - t_0)\left(1 + \int_{t_0}^{t} \frac{\gamma_2}{\gamma_1} v^{0.7} dt \Big/ (t - t_0) \right) = \gamma_1 (t - t_0)\left(1 + \frac{\gamma_2}{\gamma_1} E[v^{0.7}](t) \right) \tag{A.9}$$

where $E[v^{0.7}](t)$ is the mean value of $v^{0.7}$ in the interval $[t_0, t]$. For $t >> t_0$ we assume that $E[v^{0.7}](t)$ can be considered to be approximately constant so that $\tau = \xi_1 t + \xi_2$, where ξ_1 and ξ_2 are constants, and the solution in Eq. (A.8) for large enough t becomes:

$$T_s(t) \approx \int_{t_0}^{t} e^{-B_0(t-s)} \sum_{i=1}^{N} A_i P_i(s) ds + D \tag{A.10}$$

Here we have incorporated the constants ξ_1 and ξ_2 in the other unknown constants and we have dropped the initial condition constant due to the reasons explained above.

The solution in Eq. (A.10) is an approximate equation for calculation of the surface temperature. However, in our applications most often not the actual surface temperature that has been measured. It is in most cases the radiance, L, that has been measured with some sensor in a particular wavelength band. If the measured radiance has been corrected for atmospheric absorption between the considered surface and the sensor, the radiance detected by the sensor is a sum of thermal radiation emitted from the surface, L_{emitt}, and radiation reflected from the surface, L_{refl}. The emitted radiance can be assumed to be proportional to the radiation emitted from a blackbody at the same temperature (constant of proportionality is the emissivity) in the wavelength band. However, we will assume a linear correlation between the radiance detected and the surface temperature: $L_{emitt} = \eta_1 + \eta_2 T_s$. This is actually a rather good approximation when considering the wavelength band 8-12 µm and when the temperatures are normal ground level temperatures as can be seen in Figure 17.

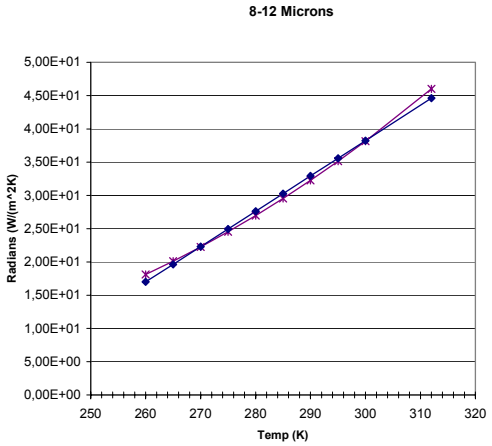

Figure 17 Blackbody radiance in the wavelength band 8-12 µm versus temperature. Included in the figure is also a linear fit to the blackbody radiance.

Furthermore, we assume that the reflected part of the detected radiation is proportional to E_{sky}, E_{sun} or a linear combination of these. In the model we actually let $L_{refl} \approx f_1 E_{sky} + f_2 E_{sun}$. Here we actually assume that the surface is diffuse and the validity of this approximation depends strongly on which wavelength band that is considered. In the long wave IR band, 8-12, we can in many cases expect a reasonable proportionality between L_{refl} and E_{sky} for a diffuse surface. In any case we can now, with the above assumptions, go from the equation for surface temperature, Eq. (A.10) to the following equation for radiance from the surface element:

$$L(t) \approx \int_{t_0}^{t} e^{-B_0(t-s)} \sum_{i=1}^{N} A_i P_i(s) ds + C_1 P_1 + C_2 P_2 + D \qquad \text{(A.11)}$$

where we now have two more free unknown constants C_1 and C_2.

Now we will try to derive an incremental agorithm for the radiance from Eq. (A.11). We will derive this incremental algorithm for a generalization of Eq. (A.11):

$$L(t) \approx \int_{t_0}^{t} e^{-B_0(t-s)} \sum_{i=1}^{N} A_i P_i(s) ds + \sum_{i=1}^{N} C_i P_i + D \tag{A.12}$$

We can also express this as:

$$\begin{aligned} L(t) &\approx \sum_{i=1}^{N} \int_{t_0}^{t} \left(A_i e^{-B_0(t-s)} + C_i \delta(t-s) \right) P_i(s) ds + D = \\ &= \sum_{i=1}^{N} \int_{t_0}^{t} K_i(A_i, C_i; t-s) P_i(s) ds + D \end{aligned} \tag{A.13}$$

where $K_i(A_i, C_i; t-s)$ is a transfer function for the considered system.

Consider terms in Eq. (A.12) which are of the form:

$$F_i(t) = \int_{t_0}^{t} A_i e^{-B_0(t-s)} P_i(s) ds = \int_{t-t_x}^{t} A_i e^{-B_0(t-s)} P_i(s) ds + \int_{t_0}^{t-t_x} A_i e^{-B_0(t-s)} P_i(s) ds \tag{A.14}$$

If $t - t_x << t$, $B_0 > 0$ and P_i does not change sign we have

$$\int_{t_0}^{t-t_x} A_i e^{-B_0(t-s)} P_i(s) ds = (t - t_x - t_0) A_i P_i(t_p), \tag{A.15}$$

For large $t - t_p$ we therefore have

$$F_i(t) \approx \int_{t-t_x}^{t} A_i e^{-B_0(t-s)} P_i(s) ds \tag{A.16}$$

and

$$\begin{aligned} F_i(t+\Delta t) &\approx \int_{t+\Delta t-t_x}^{t+\Delta t} A_i e^{-B_0(t+\Delta t-s)} P_i(s) ds = \\ &= e^{-B_0 \Delta t} \left[\int_{t-t_x}^{t} A_i e^{-B_0(t-s)} P_i(s) ds + \int_{t}^{t+\Delta t} A_i e^{-B_0(t-s)} P_i(s) ds - \int_{t-t_x}^{t-t_x+\Delta t} A_i e^{-B_0(t-s)} P_i(s) ds \right] \end{aligned} \tag{A.17}$$

These integrals can be discretized in several ways but we choose to make a piecewise constant approximation of the integrals. We take

$$\overline{P}_i^{t+\Delta t} = \frac{1}{2}(P_i(t+\Delta t) + P_i(t)) \tag{A.18}$$

and under the piecewise constant condition we get

$$F_i(t+\Delta t) = e^{-B_0\Delta t}\left[F_i(t) + \left(\frac{A_i}{B_0} e^{B_0\Delta t} \overline{P}_i^{\,t+\Delta t} - \frac{A_i}{B_0} \overline{P}_i^{\,t+\Delta t} \right) - \left(\frac{A_i}{B_0} e^{-B_0(t_x-\Delta t)} \overline{P}_i^{\,t-t_x+\Delta t} - \frac{A_i}{B_0} e^{-B_0 t_x} \overline{P}_i^{\,t-t_x+\Delta t} \right) \right] \tag{A.19}$$

However the last parenthesis is much smaller than the other terms and we get

$$F_i(t+\Delta t) = e^{-B_0\Delta t} F_i(t) + \frac{A_i}{B_0}(1-e^{-B_0\Delta t})\overline{P}_i^{\,t+\Delta t} \tag{A.20}$$

Now consider the terms in Eq. (A.12) which are of the form

$$G_i(t) = C_i P_i(t) \tag{A.21}$$

Rewrite this as

$$G_i(t+\Delta t) = C_i P_i(t+\Delta t) = e^{-B_0\Delta t} G_i(t) + C_i P_i(t+\Delta t) - e^{-B_0\Delta t} P_i(t) C_i \tag{A.22}$$

and we arrive at:

$$G_i(t+\Delta t) = e^{-B_0\Delta t} G_i(t) - 2e^{-B_0\Delta t} C_i \overline{P}_i^{\,t+\Delta t}(t) + C_i(1+e^{-B_0\Delta t}) P_i(t+\Delta t) \tag{A.23}$$

The constant term, D, in Eq. (A.12) can be rewritten as:

$$D = e^{-B_0\Delta t} D + D(1-e^{-B_0\Delta t}) \tag{A.24}$$

When inserting Eqs. (A.20), (A.23) and (A.24) in Eq. (A.12) we get

$$\begin{aligned} L(t+\Delta t) &= \sum_{i=1}^{N} F_i(t+\Delta t) + \sum_{i=1}^{N} G_i(t+\Delta t) + D = \\ &= e^{-B_0\Delta t}\left(\sum_{i=1}^{N} F_i(t) + \sum_{i=1}^{N} G_i(t) + D \right) + \\ &+ \sum_{i=1}^{N} \overline{P}_i^{\,t+\Delta t}\left[-e^{-B_0\Delta t}\left(\frac{A_i}{B_0} + 2C_i \right) + \frac{A_i}{B_0} \right] + \sum_{i=1}^{N} C_i(1+e^{-B_0\Delta t}) P_i(t+\Delta t) + D(1-e^{-B_0\Delta t}) \end{aligned} \tag{A.25}$$

By combining unknown constants into new ones this can be written as:

$$
\begin{aligned}
&L(t+\Delta t) = aL(t) + \sum_{i=1}^{N} b_i \overline{P}_i^{\,t+\Delta t} + \sum_{i=1}^{N} c_i P_i(t+\Delta t) + d \\
&a = e^{-B_0 \Delta t} \\
&b_i = -e^{-B_0 \Delta t}\left(\frac{A_i}{B_0} + 2C_i\right) + \frac{A_i}{B_0} \\
&c_i = C_i\left(1 + e^{-B_0 \Delta t}\right) \\
&d = D\left(1 - e^{-B_0 \Delta t}\right)
\end{aligned}
\qquad \text{(A.26)}
$$

Eq. (A.26) is the incremental algorithm, which is linear in the unknown constants a, b_i, c_i and d, and which is our end result.

We can also solve for the old constants A_i, B_0, C_i and D in terms of the new ones:

$$
\begin{aligned}
&B_0 = -\ln a / \Delta t \\
&D = d/(1-a) \\
&C_i = c_i/(1+a) \\
&A_i = \left(b_i + \frac{2a}{1+a} c_i\right) \frac{\ln a}{\Delta t} \Big/ (a-1)
\end{aligned}
\qquad \text{(A.27)}
$$

Eqs. (A.26) and (A.27) are the equations which we use for curve-fitting parameters and predicting radiance in our semi-empirical model (see Section 2).

APPENDIX B DIFFUSE FRACTION MODEL OF SKARTVEIT ET AL.

In this appendix we briefly present the equations which we use from the model for calculation of diffuse fraction of Skartveit et al., Ref 7.

The correlation for the diffuse to global horizontal irradiation quotient, $E_{sun}^{dh}/E_{sun}^{gh}$, is a function of solar elevation, θ_s, clearness index, K_c, and an hourly variability index, σ_3. The variability index is defined as the root mean square deviation between the "clear sky" index of the hour in question (ρ_0) and, respectively, the preceding (ρ_{-1}) and the succeeding (ρ_1) hour:

$$\sigma_3 = \begin{cases} \sqrt{[(\rho_0-\rho_1)^2+(\rho_0-\rho_{-1})^2]/2}, & \text{when } \rho_1 \text{ and } \rho_{-1} \text{ are both known} \\ |\rho_0-\rho_{-1}|, & \text{when either } \rho_1 \text{ or } \rho_{-1} \text{ is not known} \end{cases} \quad \text{(B1)}$$

The clear sky index is given by:

$$\rho = K_c / k_1 \quad \text{(B2)}$$

where

$$k_1 = 0.83 - 0.56e^{-0.06\theta_s}, \text{ and } \theta_s \text{ is in degrees} \quad \text{(B3)}$$

The diffuse to global horizontal irradiation quotient is given by:

$$\frac{E_{sun}^{dh}}{E_{sun}^{gh}} = \begin{cases} 1+\Delta(K_c,\theta_s,\sigma_3), & K_c \le 0.22 \\ 1-(1-d_1)(0.11\sqrt{k_{\text{mod}}}+0.15k_{\text{mod}}+0.74k_{\text{mod}}^2)+\Delta(K_c,\theta_s,\sigma_3), & 0.22 < K_c \le k_2 \\ d_2k_2(1-K_c)/[K_c(1-k_2)]+\Delta(K_c,\theta_s,\sigma_3), & k_2 < K_c \le k_{\max} \\ 1-k_{\max}(1-d_{\max})/K_c+\Delta(K_c,\theta_s,\sigma_3), & K_c > k_{\max} \end{cases} \quad \text{(B4)}$$

where

$$k_{\text{mod}} = 0.5[1+\sin(\pi(K_c-0.22)/(k_1-0.22)-\pi/2)] \quad \text{(B5)}$$

$$k_2 = 0.95k_1 \quad \text{(B6)}$$

$$d_1 = 0.07+0.046(90-\theta_s)/(\theta_s+3) \text{ for } \theta_s \ge 1.4^\circ \text{ and } d_1 = 1 \text{ otherwise} \quad \text{(B7)}$$

$$d_2 = 0.5[1+\sin(\pi(k_2-0.22)/(k_1-0.22)-\pi/2)] \quad \text{(B8)}$$

$$k_{\max} = [0.81^\alpha + d_2k_2/(1-k_2)]/[1+d_2k_2/(1-k_2)],\ \alpha = [1/\sin\theta_s]^{0.6} \quad \text{(B9)}$$

$$d_{\max} = k_2d_2(1-k_{\max})/[k_{\max}(1-k_2)] \quad \text{(B10)}$$

and

$$\Delta(K_c,\theta_s,\sigma_3)=\begin{cases}0, & K_c \le 0.14\\ -3k_L^2(1-k_L)\sigma_3^{1.3}, & 0.14 < K_c \le k_x\\ 3k_R(1-k_R)^2\sigma_3^{0.6}, & k_x < K_c \le k_x + 0.71\\ 0, & K_c > k_x + 0.71\end{cases} \quad \text{(B11)}$$

where

$$k_x = 0.56 - 0.32e^{-0.06\theta_s} \quad \text{(B12)}$$

$$k_L = (K_c - 0.14)/(k_x - 0.14) \quad \text{(B13)}$$

$$k_R = (K_c - k_x)/0.71 \quad \text{(B14)}$$

In the implementation of these equations we have chosen to calculate the variability index on an hourly basis, while the other quantities are calculated from essentially instantaneous data. This is an assumption we make that this diffuse fraction model can be used for much shorter time averages than the hourly averages assumed by Skartviet et al.

APPENDIX C EXAMPLES OF INPUT FILES

Example of an input definition file (Microsoft Excel format):

	A	B	C
1	**Description of input data**	**Input data**	**Input files for fitted parameters. Set 0 in cell C15 if parameters are fitted in the run**
2	Fit parameters (y/n):	y	
3	Perform prediction (y/n):	y	
4	Include percipitation model in calculation (y/n)	n	
5	Include latent heat in calculation (y/n)	n	
6	If latent heat give relative humidity on (soil) surface	1	
7	Give latitude of surface element	56	
8	Give longitude of surface element	15	
9	Give azimuth of surface element (outward) normal	256	
10	Give elevation of surface element normal	30	
11	Give existing directory in which to put result directory (end name with \)	C:\OPTSIGN\SEMI_EMP\SEMSIM10\	
12	Give name of directory to put results (directory will be created if it doesn't exist, end name with \) A copy of this input file is also placed there.	result\	
13	Give paths to input data files (end name with \ when used & leave blank if no data files are provided :	C:\OPTSIGN\SEMI_EMP\SEMSIM10\INPUTPANEL89\	C:\OPTSIGN\SEMI_EMP\SEMSIM10\result\
14	Give weather data file (extension .xls):	Weather8-9pahe.xls	
15	Give number of radiance measurement files and number of fitted data (.mat) files. (should be equal if both are > 0)	2	0
16	Give the names of radiance measurement files (extension .xls or .dat, column B) and/or corresponding fitted parameters (extension .mat, column C) . Leave blank if no data is provided. More lines can be added.	radpaintpahe.xls	radpaintpahe.mat
17		radfoilpahe.xls	radfoilpahe.mat
18			
19			
20			
21			

The first few rows of an example weather data input file (Microsoft Excel format):

Tid (UTC)	VINDRIKTNING	VINDHASTIGHET	LUFTTEMPERATUR	FUKT	TRYCK	NEDERBORD	SIKT (1 MIN MEDELVARDE)	EXTENSION KOEFFICIENT	SIKT (10 MIN MEDELVARDE)	EXTENSION KOEFFICIENT	NEDERBORDSTYP	NEDERBORDSINTENSITET	NEDERBORDSMANGD (REGN)	NEDERBORDSMANGD (SNO)	DIREKT VaDER	INSTRALNING (ALBEDOMETER)	MARKSTRALNING (ALBEDOMETER)	ALBEDO	INSTRALNING (PYRGEOMETER)	MARKSTRALNING (PYRGEOMETER)	STRALNINGSBALANS (EXTRA)	STRALNINGSBALANS (SCHENK)
including date	(Grader)	(m/s)	(Grader C)	(procent)	(hPa)	(ON/OFF)	(km)	(1/km)	(km)	(1/km)	(Regn/sno	(mm/h)	(mm)	(mm)	(KOD)	(W/m2)	(W/m2)	(procent)	(W/m2)	(W/m2)	(W/m2)	(W/m2)
2003-04-07 13:48	45	6,4	2,5	29,5	1018	0	6,8	0,44	6,77	0,44	NaN	0	0	0	4	403	115	28,6	-346	0	-58	-209
2003-04-07 13:49	56	5,2	2,4	29,7	1018	0	6,85	0,44	6,73	0,45	NaN	0	0	0	4	316	64,4	20,4	-140	-17	128	-212
2003-04-07 13:50	6	3,1	2,4	29,2	1018	0	6,63	0,45	6,71	0,45	NaN	0	0	0	4	382	76,4	20	-109	-5	201	-216
2003-04-07 13:51	45	2,8	2,3	30	1018	0	6,67	0,45	6,75	0,44	NaN	0	0	0	4	153	34,1	22,2	-114	-13	18,4	-350
2003-04-07 13:52	39	5	2,1	30,3	1018	0	6,57	0,46	6,78	0,44	NaN	0	0	0	4	131	27,3	20,9	-116	-18	5,6	-240
2003-04-07 13:53	23	5,9	2	30,2	1018	0	6,46	0,46	6,71	0,45	NaN	0	0	0	4	142	29,4	20,7	-117	-20	15,4	-160
2003-04-07 13:54	34	3,4	1,9	30,3	1018	0	6,2	0,48	6,59	0,46	NaN	0	0	0	4	322	67,3	20,9	-107	-2	150	-162

The first few rows of an example radiance data input file (Microsoft Excel format):

	LW
Tid (UTC)	**Vänster målad plåtpanel**
	Radians
2003-04-08 12:37	34,208115
2003-04-08 12:39	34,169064
2003-04-08 12:40	34,415474
2003-04-08 12:41	34,426988
2003-04-08 12:42	34,190778
2003-04-08 12:43	33,67605
2003-04-08 12:44	33,61356
2003-04-08 12:45	33,188063
2003-04-08 12:46	32,912119
2003-04-08 12:47	33,246459
2003-04-08 12:48	33,475414
2003-04-08 12:49	33,517099
2003-04-08 12:50	33,312426
2003-04-08 12:51	33,442565
2003-04-08 12:52	33,270512
2003-04-08 12:53	33,361648
2003-04-08 12:54	33,303305
2003-04-08 12:55	33,771478
2003-04-08 12:56	33,684153
2003-04-08 12:57	33,909973
2003-04-08 12:58	34,073618
2003-04-08 12:59	33,782398
2003-04-08 13:00	34,278353
2003-04-08 13:01	34,629671
2003-04-08 13:02	34,622642
2003-04-08 13:03	34,52573
2003-04-08 13:04	34,36757
2003-04-08 13:05	34,433632
2003-04-08 13:06	34,444782
2003-04-08 13:07	34,4335
2003-04-08 13:08	35,008585
2003-04-08 13:09	35,002257
2003-04-08 13:10	35,25155
2003-04-08 13:11	35,368348
2003-04-08 13:12	35,295908
2003-04-08 13:13	35,613768
2003-04-08 13:14	35,736979
2003-04-08 13:15	35,577817
2003-04-08 13:16	35,353167